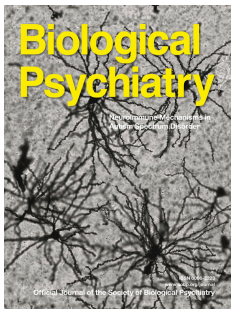
Journal Pre-proof



Social stress increases anxiety by GluA1-dependent synaptic strengthening of ventral tegmental area inputs to the basolateral amygdala

Thomas Contesse, Joana Gomes-Ribeiro, Lea Royon, Hugo Fofo, Anaelle Braine, Christelle Glangetas, Shiliang Zhang, M. Flavia Barbano, Mariano Soiza-Reilly, François Georges, Jacques Barik, Sebastian P. Fernandez

PII: S0006-3223(25)01121-7

DOI: https://doi.org/10.1016/j.biopsych.2025.04.007

Reference: BPS 15787

To appear in: *Biological Psychiatry*

Received Date: 5 September 2024

Revised Date: 17 March 2025

Accepted Date: 6 April 2025

Please cite this article as: Contesse T., Gomes-Ribeiro J., Royon L., Fofo H., Braine A., Glangetas C., Zhang S., Barbano M.F., Soiza-Reilly M., Georges F., Barik J. & Fernandez S.P., Social stress increases anxiety by GluA1-dependent synaptic strengthening of ventral tegmental area inputs to the basolateral amygdala, *Biological Psychiatry* (2025), doi: https://doi.org/10.1016/j.biopsych.2025.04.007.

This is a PDF file of an article that has undergone enhancements after acceptance, such as the addition of a cover page and metadata, and formatting for readability, but it is not yet the definitive version of record. This version will undergo additional copyediting, typesetting and review before it is published in its final form, but we are providing this version to give early visibility of the article. Please note that, during the production process, errors may be discovered which could affect the content, and all legal disclaimers that apply to the journal pertain.

© 2025 Published by Elsevier Inc on behalf of Society of Biological Psychiatry.

Social stress increases anxiety by GluA1-dependent synaptic strengthening of ventral tegmental area inputs to the basolateral amygdala

Thomas Contesse[1, 2, 3#], Joana Gomes-Ribeiro[1,2,3#], Lea Royon[1,2,3], Hugo Fofo[1,2,3], Anaelle Braine[4], Christelle Glangetas[4], Shiliang Zhang[5], M. Flavia Barbano[6], Mariano Soiza-Reilly[7], François Georges[4], Jacques Barik[1,2,3*] and Sebastian P. Fernandez[1, 2,3*]

1 Université Côte d'Azur, Nice, France.

2 Institut de Pharmacologie Moléculaire & Cellulaire, CNRS UMR7275, Valbonne, France.

3 Inserm U1323

4 Université de Bordeaux, CNRS, IMN, UMR 5293, F-33000 Bordeaux, France

5 Confocal and Electron Microscopy Core, National Institute on Drug Abuse, National Institutes of Health, Baltimore, MD, 21224, USA

6 Integrative Neuroscience Research Branch, National Institute on Drug Abuse, National Institutes of Health, Baltimore, MD 21224, USA

7 Instituto de Fisiología, Biología Molecular y Neurociencias (IFIBYNE), Consejo Nacional de Investigaciones Científicas y Técnicas (CONICET), Facultad de Ciencias Exactas y Naturales, Universidad de Buenos Aires, Buenos AiresC1428EGA, Argentina.

[#] These authors contributed equally; * Co-last authors

Correspondence author: S.P.F. (fernandez@ipmc.cnrs.fr) or J.B. (barik@ipmc.cnrs.fr)

Running tittle: **Social Stress Elevates Anxiety via VTA-BLA Synaptic Strengthening**

Keywords: ventral tegmental area, amygdala, glutamatergic, AMPA receptors, anxiety, social stress

Journal Pre-proof

ABSTRACT

BACKGROUND: Brain defensive mechanisms evolved to maintain low levels of state anxiety. However, risk factors such as stress exposure shifts activity within defensive circuits, resulting in increased anxiety. The amygdala is a crucial node for maintaining adaptive anxiety levels, and amygdala hyperactivity can lead to pathological anxiety through mechanisms that are not well understood.

METHODS: We used chronic social defeat stress (CSD) in mice. We combined anatomical tracing methods, patch-clamp recordings and optogenetics to probe how synaptic inputs from the ventral tegmental area (VTA) to the basolateral amygdala (BLA) are affected by CSD. We performed in vivo fiber photometry recordings to track inputs onto basolateral amygdala. Array tomography and electron microscopy were used to unravel the structural composition of VTA-BLA synapses.

RESULTS: We identified the VTA as a source of glutamatergic inputs to the BLA potentiated by stress. In turn, inputs from mPFC were not potentiated. BLA-projecting VTA glutamatergic neurons are activated by social stress, increasing their excitability and synaptic strength. In vivo potentiation of VTA glutamatergic inputs in the BLA is sufficient to increase anxiety. We showed that stress-induced synaptic strengthening is mediated by insertion of GluA1-containing AMPA receptors. Impeding GluA1 subunit trafficking in BLA neurons with VTA upstream inputs prevents stress-induced increase in synaptic firing and anxiety.

CONCLUSIONS: Potentiation of VTA inputs increases synaptic integration, enhancing amygdala activity and promoting maladaptive anxiety. Understanding the impact of amygdala hyperactivity could lead to targeted therapies, restoring circuit balance and offering new precision medicine approaches for anxiety disorders.

Journal Pre-proof

Anxiety is an adaptive response to threats, but when exaggerated, it negatively affects mental well-being (1,2). Anxiety disorders, the most prevalent psychiatric conditions, impose significant individual and societal burdens(3–5). Pathological anxiety is linked to heightened activity in fear circuits, particularly the amygdala, which evaluates emotional significance and predictive value of stimuli (2,6,7). Disruptions in the balance of excitatory and inhibitory signals in amygdala principal neurons can lead to heightened emotional responses (10). Hyperactivity in the amygdala is central to anxiety disorders, with imaging showing increased reactivity in patients (11–13,15,16). However, the precise cellular mechanisms responsible for the increased activity of amygdalar principal neurons remain unclear. Understanding these mechanisms is crucial for both clinical insights and therapeutic advancements. Extensive research has shown that stress—a major contributor to anxiety—induces significant morphological changes in the amygdala, such as increased dendritic branching and spine density in principal neurons (17–19). These findings highlight the potential role of glutamatergic inputs in driving amygdala hyperactivity and anxiety-related behaviors.

The amygdala receives excitatory inputs from multiple brain structures including cortical and subcortical regions (8,9). Excitatory inputs from the prefrontal cortex region are important for fear processing (20–22). Yet, anatomical studies indicate the presence of non-cortical excitatory inputs, notably glutamatergic neurons in modulatory regions (23–26). Recent research has linked a subpopulation of VTA VGluT2-expressing neurons to innate emotional regulation to threats (27,28). Neuroanatomical studies have revealed that glutamate neurons within the VTA extensively innervate the amygdala (29) although the precise impact of this innervation on amygdalar function remains to be fully elucidated.

This study investigated the role of VTA glutamatergic neurons in amygdala hyperactivity following chronic stress. Using anatomical, electrophysiological, optogenetics, and fiber photometry techniques in a social defeat model, we found that stress strengthens VTA-amygdala

connections, increasing synaptic firing in amygdala principal neurons. In contrast, mPFC glutamatergic inputs were unaffected. This synaptic potentiation is driven by increased GluA1-containing AMPA receptors at VTAGlu-BLA synapses, ultimately promoting anxiety.

METHODS AND MATERIALS

Experimental model and subject details.

We used C57BL/6J and CD1 mice, vGAT-CRE mice and VGluT2-CRE mice (27). Transgenic mice were heterozygous and backcrossed on a C57BL/6J background. Mice were enriched housed 4–5 mice per cage on a 12 h/12 h light/dark cycle with lights on from 8:00 a.m to 8:00 p.m, with free access to food and water. All mice used in behavioural experiments were pre-handled daily for 1 week during 5 minutes sessions for 1 week before each test to limit any stress induced by the manipulator. In addition, during these pre-handling sessions, animals from in vivo optogenetic cohorts were habituated to being connected to laser cables for 20 min daily.

All behavioral tests, ex-vivo and in-vivo recordings were performed on adult mice that were at least 2 months old and littermates were used as controls. All the experiments were performed in accordance with the ARRIVE guidelines. All procedures were in accordance with the recommendations of the European Commission (2010/63/EU) for care and use of laboratory animals and approved by the French National Ethical Committee.

Chronic social defeat

The CSD stress paradigm was performed as previously (30). WT, transgenic mice, and their respective control littermates were subjected to 10 consecutive days of social defeat by former CD1 breeder male mice. Each experimental mouse faced a new CD1 every day and sessions of defeat were limited to a maximum of 5 min. Mice were then maintained in sensory, but not

physical, contacts with the dominant male through a semi-permeable barrier. Undefeated mice (Naive) were not confronted with a dominant male but lived in similar housing conditions, separated by a semi-permeable barrier. For social defeat of female mice, cotton swabs were used to apply urine of male CD1 around the vaginal orifice, tail and lower back of females mice and were then placed in a resident CD1 home cage as we previously described (31).

Details on behavioral testing can be found in the Supplement.

Stereotaxic virus injections and optical fiber implantations.

Stereotaxic injections were performed using a stereotaxic frame (Kopf Instruments) under general anaesthesia with xylazine and ketamine (10 mg/kg and 150 mg/kg, respectively). The injection rate was set at 100nl/min. Anatomical coordinates were adjusted from Paxinos and were as follows: VTA AP: -2.9mm, ML:±0.6mm, DV:-4.7mm; BLA AP:-0.9mm, ML:±3.22mm, DV:-4.6mm. Detailed information appears in the Supplement concerning in vivo optogenetic manipulation and fiber photometry recordings.

***Ex-vivo* patch-clamp recording.**

Mice were anesthetized (ketamine 150 mg/kg / xylazine 10 mg/kg) and transcardially perfused with aCSF for slice preparation. For VTA recordings, horizontal 250 µm slices were obtained in bubbled ice-cold 95% O2/5% CO2 aCSF containing (in mM): KCl 2.5, NaH2PO4 1.25, MgSO4 10, CaCl2 0.5, glucose 11, sucrose 234, NaHCO3 26. Slices were then incubated in aCSF containing (in mM): NaCl 119, KCl 2.5, NaH2PO4 1.25, MgSO4 1.3, CaCl2 2.5, NaHCO3 26, glucose 11, at 37°C for 1 h, and then kept at room temperature. For amygdala recordings, coronal

250 µm sections were obtained using the same solutions. Detailed information concerning electrophysiology protocols used and single-cell PCR appear in the Supplement.

Microscopy.

Details concerning microscopy experiments for histology, c-Fos counting, array tomography quantification and electron microscopy appear in the Supplement.

Data analysis

Data were analysed using Prism (GraphPad, U.S.A.). Normality of the distribution was first tested using a Kolmogorov-Smirnov test. Depending of the number of groups and the results of the normality test, groups were then compared using a Student t-test, U of Mann-Whitney, or two-way analyses of variance (ANOVA) followed by post hoc Sidak's test. Data in the figures are presented as mean ± SEM. Statistical significance was conventionally established at *p<0.05, **p<0.01, ***p<0.001.

Journal Pre-proof

RESULTS

Chronic social stress increases anxiety and synaptic firing of basolateral amygdala principal neurons

To study the mechanisms that results in increased anxiety male and female mice were subjected to 10 days of chronic social defeat (CSD), followed by behavioral tests measuring anxiety and by patch-clamp recordings (Figure 1A). Stressed mice showed decreased exploration of open arms in the O-maze compared to control subjects (Figure 1B). In the open field, CSD mice ventured

less to the center area but the total distance travelled was similar for both groups (Figure 1C). These results showed that CSD promotes anxious behaviors in mice without altering locomotor function. After the behavioral tests, mice were used for patch-clamp recordings in acute brain slices (Figure 1D). Principal (glutamatergic) cells of the basolateral amygdala (BLA) participate in anxiety modulation(32). We identified this neuronal population by morphological as well as described electrophysiological properties (33,34). Patch-clamp recordings showed that CSD exposure did not alter passive membrane properties such as resting membrane potential (RMP) or membrane resistance (Rm) nor their excitability in response to increasing current steps (Figure 1D). However, CSD did significantly increase the frequency, but not the amplitude, of spontaneous excitatory post-synaptic currents (sEPSC) (Figure 1E), suggesting an increased glutamatergic terminal release onto amygdala principal neurons. To ascertain how synaptic inputs modulate output firing activity in these cells, we applied a protocol of synaptic stimulation to evoke action potentials. In this protocol, BLA neurons from stressed mice showed a significant higher probability of action potential firing compared to control mice (Figure 1F). Importantly, both male and female mice subjected to CSD showed similar changes in anxiety levels in the O-maze, and increased firing probability in patch-clamp recordings compared to controls (Figure S1A). In turn, mice subjected to a single defeat session do not show elevated anxiety levels 24h post-acute defeat in both the O-maze and the open field tests (Figure S1A). In acute slices prepared from these mice, BLA principal neurons did not show significant changes in synaptic firing (Figure S1B). These results demonstrate that exposure to chronic stress increases anxiety in mice, presumably by increasing glutamatergic release and synaptic firing of basolateral amygdala principal neurons.

VTA glutamatergic neurons are functionally connected to BLA principal neurons

Recent studies suggest VTA glutamatergic neurons modulate threat responses, prompting us to explore their role in stress-induced anxiety via amygdala projections. We characterized VTAGlu neuron connectivity with amygdala nuclei anatomically and functionally. We expressed ChR2-mCherry, and found that axonal projections were most abundant in the BLA and centromedial amygdala (Figure S2A). Ex vivo patch-clamp recordings with blue light stimulation of VTAGlu terminals showed the highest opto-stimulation responses and post-synaptic current amplitudes in the BLA (Figure S2B-C), identifying it as the primary target of VTAGlu projections.

Focusing on the BLA, we showed that in voltage-clamp recordings, short (5ms) blue light pulses resulted in inward currents with an onset delay of 2.41±0.17ms (mean±SEM), suggesting monosynaptic connectivity (35). These inward responses were blocked by application of the AMPA receptor antagonist DNQX, demonstrating that VTAGlu axons release glutamate and activate post-synaptic AMPA receptors (Figure 2A). Optogenetic activation of VTAGlu terminals was sufficient to elicit action potentials in BLA principal neurons (Figure 2A). We suctioned the cytoplasm of a subset BLA recorded neurons, and conducted single-cell RT-PCR for glutamatergic and GABAergic markers. Most recorded neurons (6 out of 7) expressed the glutamatergic vesicular transporter type 1, consistent with principal glutamatergic neurons (Figure 2B). Activation of VTAGlu terminals within the BLA elicited a significant increase in the number of cFos+ cells, confirming a functional connection in vivo (Figure S3).

We next analysed the characteristics of VTAGlu projections in the BLA by confocal microscopy and immuno-electron microscopy. Taking advantage of CaMKII's predominant expression in VTAGlu neurons, we injected AAV-CaMKII-ChR2-mCherry into the VTA and AAV-DIO-YFP into the BLA of VGluT1-Cre mice to label glutamatergic populations in both regions (Figure 2C). A subset of VTA dopamine neurons also expresses CaMKII (36), however we minimized this confounding factor by combining axon labeling with detection of VGluT2 expression. Using quadruple fluorescent immunolabeling, we found that mCherry varicosities containing VGluT2

(derived from the VTAGlu neurons) contacted VGluT1 (eYFP-positive) cell bodies or dendrites in the BLA (Figure 2D). By electron microscopy, we confirmed that mCherry-labeled varicosities corresponded to axon terminals. By triple immuno-electron microscopy, we found that mCherry axon terminals containing VGluT2 from the VTA established asymmetric (putative excitatory) synapses on VGluT1 (eYFP-positive) dendrites in the BLA (Figure 2E). Altogether, this evidence demonstrates that VTAGlu neurons are functionally connected to BLA principal neurons.

VTA glutamatergic neurons are activated by social stress

To determine if VTAGlu neurons projecting to the BLA contribute to anxiety after CSD, we first tested their activation by social stress. Using a retrograde Cre-dependent tracer in the BLA of VGluT2-Cre mice, we found BLA-projecting glutamatergic neurons primarily in the medial VTA, with minimal co-expression of the dopaminergic marker TH (Figure 3A). Additionally, we observed that the majority of BLA-projecting neurons were located in the anterior VTA (Figure S4). Using the same viral strategy, cFos co-immunostaining revealed increased activation of BLA-projecting VTAGlu neurons by acute defeat (Figure 3B). Since cFos experiments only provided histological evidence, it remained unclear if these neurons actively transmit social stress information. Thus, we conducted fiber photometry recordings to assess their response to defeat stress. We expressed the calcium indicator GCAMP8m in VTAGlu neurons, implanted fibers over the VTA, and exposed mice to a defeat session. Each aggressor attack triggered a transient Ca2+ increase in VTAGlu neurons (Figure 3C). Using whole-cell patch-clamp recordings from CSD and control mice, we observed that exposure to CSD produced a significant increase in excitability in VTAGlu→BLA neurons (Figure 3D). These findings suggest VTAGlu neurons are activated by social stress and undergo maladaptive changes with chronic exposure, heightening glutamatergic input to the BLA and promoting anxiety.

CSD stress specifically potentiates VTA-BLA synapses

BLA neurons receive different cortical and subcortical glutamatergic inputs (37). In particular, the medial prefrontal cortex (mPFC) is an upstream regulator of amygdala activity involved in emotional regulation(38,39). We expressed GCAMP8f in BLA neurons receiving inputs from the mPFC, and conducted photometry recordings over the BLA combined with stimulation of either the mVTA or the mPFC (Figure 4A and 4B). Electrical stimulation of the mPFC in burst-like or continuous patterns (10 or 20Hz), produced strong increases in Ca2+ activity in the BLA (Figure 4C). Interestingly the same population of neurons also responded to electrical stimulation in the medial VTA, where the vast majority of glutamatergic neurons are located (Figure 4D). These results suggest that BLA neurons receive convergent excitatory inputs from the mPFC and the mVTA. To corroborate this hypothesis, we used a double opsin strategy to selectively activate glutamatergic inputs from these two regions (Figure S5A). Patch-clamp recordings were conducted in BLA principal neurons, and light pulses of 470nm or 590nm were used to activate channelrhodopsin-expressing fibers from the mPFC or chrimson-expressing fibers from the VTA (Figure S5A). Most BLA neurons responded with an inward current to both light stimulations (12/16 recorded neurons), consistent with both inputs converging on the same neurons. Inward current responses from PFC inputs were generally greater in amplitude and were followed by a large outward phase, which was not seen in VTA inputs (Figure S5B).

We expressed channelrhodopsin in mPFCGlu or VTAGlu neurons and prepared brain slices from CSD or control mice (Figure 4E and 4F). Patch-clamp recordings were conducted in BLA principal neurons combined with blue light stimulation. We assessed the ratio of AMPAR to NMDAR mediated currents recorded at +40mV, using pharmacological blockers. CSD increased the AMPAR/NMDAR ratio compared to control at VTA-BLA but not mPFC-BLA synapses (Figure 4E

and 4F). These findings reveal the VTA as a subcortical glutamatergic input to BLA neurons, and showed that CSD results in increased glutamatergic drive from the VTA, but not the mPFC.

CSD enhances trafficking of AMPAR favoring insertion of GluA1 subunits and synaptic firing of BLA neurons

Increases of AMPAR/NMDAR ratio have been attributed to insertion of AMPA-R in the cell membrane, oftentimes accompanied by changes in their subunit composition (40–42). Using optogenetic stimulation of VTAGlu fibers, we obtained I-V curves of isolated AMPAR currents in VTAGlu-BLA synapses (Figure 5A). CSD produced an increase in inward rectification, i.e. higher current amplitudes in hyperpolarised compared to depolarised potentials (Figure 5B). The resulting rectification index was significantly increased after CSD (Figure 5B). Thus, CSD could increase GluA1 trafficking producing GluA2-lacking AMPA receptors with strong inward rectification (43,44). We next assessed how this synaptic rearrangement could impact the firing of BLA principal neurons (Figure 5AB). Experiments were conducted in current-clamp mode without glutamatergic receptor antagonists. Optogenetic activation of VTAGlu terminals at 20 or 50Hz resulted in less than 20% probability of generating action potentials in BLA principal neurons from control mice (Figure 5C and 5D). In CSD mice, the same protocol reached a significantly higher probability of action potential firing (Figure 5C and 5D). We used the same strategy to optogenetically stimulate mPFC glutamatergic inputs while recording BLA principal neurons (Figure S6A-C). Optogenetic activation of mPFC axonal terminals was sufficient to induce action potential firing at both 20 and 50Hz, however firing probability was not changed in slices from CSD mice (Figure S6D).

We obtained structural evidence to test whether CSD could increase the number of AMPAR containing the GluA1 subunit using quantitative high-resolution array tomography. We labelled

VTAGlu axons with ChrimsonR-tdTomato, and obtained ultrathin serial sections of the BLA. In CSD mice, we observed significantly more associations between VTAGlu axon terminals and AMPAR GluA1 in the BLA (Figure 5DE). This increment was not due to a CSD-induced change in the abundance of AMPAR GluA1 subunits. The total amount of VTAGlu inputs found in the BLA was increased but effect did not reach statistical significance (Figure 5E). In the same set of serial sections, we evaluated if cortical synapses also underwent similar adaptations. We counted double-stained puncta for Vglut1 and Syn, as proxy for cortical inputs, in apposition to AMPAR GluA1 subunits, and did not find significant differences between sections from control and CSD mice (Figure S7). This is in line with experiment showing that CSD does not potentiate mPFC inputs onto BLA principal neurons, nor does it change they capacity to induce action potentials. And with previous studies showing that chronic stress can produce significant remodelling of dendritic arrangement in the amygdala, in a input-specific manner (19). Overall, these data suggest that CSD potentiates VTAGlu synapses onto BLA principal neurons by increasing the abundance of postsynaptic GluA1-containing AMPARs. This synaptic reorganisation increases the efficacy of this input to depolarise BLA neurons into discharging action potentials.

Journal Pre-proof

In vivo optogenetic control of VTAglu→BLA circuit bidirectionally modulates anxiety

We posed the hypothesis that CSD potentiation of VTAglu→BLA synaptic could have a causal connection to increased anxiety. We performed optogenetic stimulation of this circuit in vivo during 5 days (Figure 6A). The next day, animals were placed on an O-maze and allowed to freely explored for 5min. We observed that mice with optogenetic stimulation of VTAGlu inputs ventured significantly less and spent less time into the open arms of the maze, suggesting increased anxiety, without changes in locomotor activity (Figure 6B). Mice were then used for ex vivo patch-clamp recordings after behaviour. BLA principal neurons receiving VTAGlu inputs showed significantly increased AMPAR/NMDAR ratio suggesting synaptic potentiation (Figure 6C).

Additionally, we observed increased inward rectification in VTAGlu inputs from animals expressing ChR2 compared to controls (Figure 6D), indicative of GluA2-lacking receptors, presumably by incorporation of GluA1 subunits. These results evidenced that strengthening synaptic inputs from the VTA in the BLA is sufficient to increase anxiety.

We tested whether inhibiting the VTAGlu→BLA circuit could blunt anxiety induced by CSD. We expressed halorhodopsin in VTAGlu neurons and implanted optic fibers over the BLA. Mice underwent behavioral assessments before and after CSD, followed by patch-clamp recordings (Figure S8A). During CSD, yellow light (595nm) was delivered to activate halorhodopsin. In the O-maze, control mice showed reduced open arm exploration after CSD, while NpHR mice spent more time exploring the open arms without changes in locomotion (Figure S8B). Patch-clamp recordings of BLA principal neurons revealed decreased firing probability in CSD mice with NpHR expression (Figure S8C). These results suggest that inhibiting VTAGlu→BLA synapses reduces stress-induced anxiety by decreasing BLA neuron firing.

Trafficking of AMPA GluA1 receptor subunits

To test the hypothesis that GluA1 subunit incorporation drives stress-induced mal-adaptions in VTAGlu inputs and anxiety, we used an intersectional virus strategy. We designed a virus to express the carboxyl cytoplasmic tail of the GluA1 subunits, fused with mCherry, in BLA neurons that received projections from the VTA (Figure 7AB). This peptide has previously been shown to block trafficking of endogenous GluA1 subunits in a dominant-negative manner(45,46). Expression of GluA1ct blocking peptide in BLA neurons with VTA inputs, prevented the increase in anxiety in response to social stress, as depicted by the time spent exploring the open arms of the O-maze (Figure 7C). In the open field, defeated mice with GluA1ct expression spent more time in the center, though this increase was not statistically significant. Notably, locomotor activity

remained unchanged (Figure 7D). Patch-clamp recordings were conducted in targeted BLA neurons after behaviour. Blocking GluA1 trafficking did not affect basic membrane properties such as resting potential and membrane resistance (Figure 7E), nor did affect discharge frequency in response to current injections (Figure S9A). We did not observe significant differences in the frequency or amplitude of sEPSC (Figure S9B), nor in paired-pulse ratio of electrical stimulation responses (Figure S9C). Ratios between AMPAR and NMDAR responses were smaller in GluA1ct neurons, but this effect was not statistically significant (Figure S9D). However, when we tested synaptic input integration, we observed that GluA1ct-mCherry expression significantly decreased BLA neurons synaptic firing after CSD compared to control (Figure 7F). Overall, these results showed that stress-induced anxiety, is mediated by integration of GluA1-containing AMPARs in a subset of BLA neurons receiving VTA inputs.

DISCUSSION

Anxiety requires the continuous detection and evaluation of environmental stimuli to generate appropriate motor, autonomic and hormonal responses. Coordinated activity within the amygdala subnuclei is pivotal in processing sensory inputs and identifying them as aversive or potentially dangerous(1,47,48). Here, we show that VTA glutamatergic projections favour connectivity to the central and basolateral parts of the amygdala, both regions previously associated with anxiety regulation(8,9). The BLA is an integrative hub receiving inputs from many brain regions, and serving roles in processing of reward and aversion via functionally distinct cell-types and projections (49). It is composed mostly of principal glutamatergic neurons (90%), intermingled by GABAergic interneurons (50,51). Many studies have shown the presence of anxiety-regulating neurons in the BLA (32,52,53), and pathological disruption of BLA activity has been linked with increased anxiety (6,7,11). Exposure to several stressors has been shown to increase innate anxiety and conditioned fear responses, and to increase the activity and responsiveness in

basolateral amygdala neurons(11,17). Stress induces significant structural changes in amygdala neurons, particularly hypertrophy in the BLA, with increased spine density and dendritic branching in BLA principal neurons after acute and chronic stress (18,54). Since spines serve as locations for glutamatergic synapses, they have the capacity to control the extent of excitatory neurotransmission affecting overall excitability. We observed that VTAGlu→BLA inputs were potentiated after CSD, but not in mPFCGlu inputs. A recent study found no changes in post-synaptic function in mPFC inputs onto BLA principal neurons after chronic restraint stress (55). However, the authors did find increased presynaptic plasticity favouring glutamatergic release onto BLA neurons (55). In our study, targeted BLA neurons were activated by VTA and PFC electrical stimulation, and optogenetic-assisted patch-clamp recordings confirmed that these inputs may converge in the same neuronal population. However, alterations in post-synaptic functions appear to be restricted to specific synapses, a phenomenon described in other regions (56,57).

Glutamatergic synaptic plasticity has been extensively studied in amygdala regions in the context of fear conditioning and fear extinction(9). The LA and the BLA play an important role during the formation of Pavlovian CS-US associations, involving a considerable rearranging of both NMDA and AMPA receptors (9,58). Deletion of AMPAR GluA1 subunits or blocking post-synaptic trafficking and insertion into LA principal neurons affects associative fear learning (43,59). Indeed, adaptive regulation of GluA1 AMPARs subunits plays a crucial role in central synaptic plasticity but has also been implicated in pathological conditions such as addiction, alcohol abuse and pain (40,60,61). Stress exposure can also alter the expression and subcellular localisation of GluA1 subunits in several limbic regions including the amygdala (42,62). Here, we showed that CSD increased the availability of GluA1 subunits in VTA→BLA principal neurons, and that blocking this insertion is sufficient to prevent the behavioural sequalae of stress. Thus, mal-adaptive increased

expression of GluA1 subunits enhances AMPAR signalling and strengthened synaptic firing and neuronal excitability, promoting anxiety behaviours.

The VTA has a canonical role in reward processing and goal-directed behaviour, mainly through its dopaminergic projections to the nucleus accumbens(63,64). Recent studies have shown that the VTA also plays a role in signalling aversion, and that subpopulations of neurons in this area are readily excited by aversive events such as a footshock, airpuff or even predator-like stimuli (27,64). This functional divergence could arise from the unique properties in distinct target-specific cell populations within the VTA. Anatomical tracing studies in mice have consistently shown that VTA neurons abundantly innervate the amygdala(29). Recent studies focusing on VTADA circuits to the amygdala revealed a role in anxiety regulation (65,66). Concerning VTA glutamatergic population, these neruons are activated by aversive stimuli (27,28), including attacks from conspecifics as we show here. Recent studies have shown that activation of VTAGlu neurons is necessary for the expression of defensive behaviours, potentially mediated by projections to the amygdala(28,67). Additionally, we have recently implicated the VTA in the expression of freezing fear responses, serving as a hub between upstream GABAergic inputs from the brainstem, and outputs to the amygdala nuclei (68). These data extend the role of the VTA beyond reward processing, demonstrating a primordial role in interpreting environmental threatening stimuli and trigger appropriate defensive responses, extending beyond the dopaminergic population. Environmental challenges producing lasting mal-adaptation on this circuit are bound to affect detection, value and stress responses to threatening stimuli. We show here that chronic stress exposure produces overactivation of the VTAGlu→BLA circuit, promoting increased avoidance of open arms, indicative of high anxiety.

Journal Pre-proof

ACKNOWLEDGMENTS AND DISCLOSURES

We are grateful to Julius Zhu, Manuel Mameli and Imane Moutkine for their help to obtain GluA1ct plasmids. We thank the staff from IPMC animal facilities for their technical support, and the members of the Physiopathology of Neuronal Circuits team for helpful discussions and technical advice. This work was supported by the Centre National de la Recherche Scientifique (CNRS), the Université Côte d'Azur, and the Agence Nationale de la Recherche (ANR-20-CE16-0014) to SPF and FG. Additional support by the French government through the France 2030 investment plan managed by the National Research Agency (ANR), as part of the Initiative of Excellence of Université Côte d'Azur under reference number ANR-15-IDEX-01, and The Collegium of Advanced Studies, and National Cancer Institute IReSP (SPAV1-23-005) to JB. The Fédération pour la Recherche sur le Cerveau and Rotary—Espoir en Tête, the Fondation pour la Recherche Médicale (FRM DEQ20180339159 and FRM EQU202403018036) to JB. TC is a recipient fourth-year Ph.D. fellowship from the Fondation pour la Recherche Médicale (FDT202106012968). LR is a recipient of a Ph.D. fellowship from the Fondation pour la Recherche Médicale (FDT202404018356). Experiments done by FB and SZ were supported by the Intramural Research Program of the National Institute on Drug Abuse (NIDA/NIH). We acknowledge the resources and services provided by the Histology and Imaging Core, NIDA IRP (NIH).

The authors report no biomedical financial interests or potential conflicts of interest.

Supplement Description:
Supplement Methods, Discussion, Figures S1-S9, Table S1

REFERENCES

1. McNaughton N, Corr PJ (2004): A two-dimensional neuropsychology of defense: fear/anxiety and defensive distance. *Neurosci Biobehav Rev* 28: 285–305.

2. Roozendaal B, McEwen BS, Chattarji S (2009): Stress, memory and the amygdala. *Nat Rev Neurosci* 10: 423–433.

3. Yang X, Fang Y, Chen H, Zhang T, Yin X, Man J, *et al.* (2021): Global, regional and national burden of anxiety disorders from 1990 to 2019: results from the Global Burden of Disease Study 2019. *Epidemiology and Psychiatric Sciences* 30: e36.

4. Santomauro DF, Herrera AMM, Shadid J, Zheng P, Ashbaugh C, Pigott DM, *et al.* (2021): Global prevalence and burden of depressive and anxiety disorders in 204 countries and territories in 2020 due to the COVID-19 pandemic. *The Lancet* 398: 1700–1712.

5. Stein DJ, Scott KM, de Jonge P, Kessler RC (2017): Epidemiology of anxiety disorders: from surveys to nosology and back. *Dialogues Clin Neurosci* 19: 127–136.

6. McEwen BS, Bowles NP, Gray JD, Hill MN, Hunter RG, Karatsoreos IN, Nasca C (2015): Mechanisms of stress in the brain. *Nat Neurosci* 18: 1353–1363.

7. Zhang W-H, Zhang J-Y, Holmes A, Pan B-X (2021): Amygdala Circuit Substrates for Stress Adaptation and Adversity. *Biological Psychiatry* 89: 847–856.

8. Janak PH, Tye KM (2015): From circuits to behaviour in the amygdala [no. 7534]. *Nature* 517: 284–292.

9. Duvarci S, Pare D (2014): Amygdala Microcircuits Controlling Learned Fear. *Neuron* 82: 966–980.

10. Hariri AR, Holmes A (2015): Finding translation in stress research. *Nat Neurosci* 18: 1347–1352.

11. Rosenkranz JA, Venheim ER, Padival M (2010): Chronic Stress Causes Amygdala Hyperexcitability in Rodents. *Biological Psychiatry* 67: 1128–1136.

12. Phan KL, Fitzgerald DA, Nathan PJ, Tancer ME (2006): Association between Amygdala Hyperactivity to Harsh Faces and Severity of Social Anxiety in Generalized Social Phobia. *Biological Psychiatry* 59: 424–429.

13. Fatahi Z, Zibaii MI, Haghparast A (2017): Effect of acute and subchronic stress on electrical activity of basolateral amygdala neurons in conditioned place preference paradigm: An electrophysiological study. *Behavioural Brain Research* 335: 19–25.

14. Ferry B (Ed.) (2012): *The Amygdala - A Discrete Multitasking Manager*. InTech. https://doi.org/10.5772/2973

15. Etkin A, Wager TD (2007): Functional Neuroimaging of Anxiety: A Meta-Analysis of Emotional Processing in PTSD, Social Anxiety Disorder, and Specific Phobia. *Am J Psychiatry* 164: 1476–1488.

16. Shin LM, Wright CI, Cannistraro PA, Wedig MM, McMullin K, Martis B, *et al.* (2005): A Functional Magnetic Resonance Imaging Study of Amygdala and Medial Prefrontal Cortex Responses to Overtly Presented Fearful Faces in Posttraumatic Stress Disorder. *Arch Gen Psychiatry* 62: 273–281.

17. McEwen BS, Nasca C, Gray JD (2016): Stress Effects on Neuronal Structure: Hippocampus, Amygdala, and Prefrontal Cortex. *Neuropsychopharmacology* 41: 3–23.

18. Vyas A, Jadhav S, Chattarji S (2006): Prolonged behavioral stress enhances synaptic connectivity in the basolateral amygdala. *Neuroscience* 143: 387–393.

19. Zhang W-H, Liu W-Z, He Y, You W-J, Zhang J-Y, Xu H, *et al.* (2019): Chronic Stress Causes Projection-Specific Adaptation of Amygdala Neurons via Small-Conductance Calcium-Activated Potassium Channel Downregulation. *Biol Psychiatry* 85: 812–828.

20. Jercog D, Winke N, Sung K, Fernandez MM, Francioni C, Rajot D, *et al.* (2021): Dynamical prefrontal population coding during defensive behaviours. *Nature* 595: 690–694.

21. Dejean C, Courtin J, Rozeske RR, Bonnet MC, Dousset V, Michelet T, Herry C (2015): Neuronal Circuits for Fear Expression and Recovery: Recent Advances and Potential Therapeutic Strategies. *Biological Psychiatry* 78: 298–306.

22. Likhtik E, Stujenske JM, Topiwala MA, Harris AZ, Gordon JA (2014): Prefrontal entrainment of amygdala activity signals safety in learned fear and innate anxiety. *Nat Neurosci* 17: 106–113.

23. Belmer A, Beecher K, Jacques A, Patkar OL, Sicherre F, Bartlett SE (2019): Axonal Non-segregation of the Vesicular Glutamate Transporter VGLUT3 Within Serotonergic Projections in the Mouse Forebrain. *Front Cell Neurosci* 13. https://doi.org/10.3389/fncel.2019.00193

24. McFadyen J (2019): Investigating the Subcortical Route to the Amygdala Across Species and in Disordered Fear Responses. *J Exp Neurosci* 13: 1179069519846445.

25. Fu J-Y, Yu X-D, Zhu Y, Xie S-Z, Tang M-Y, Yu B, Li X-M (2020): Whole-Brain Map of Long-Range Monosynaptic Inputs to Different Cell Types in the Amygdala of the Mouse. *Neurosci Bull* 36: 1381–1394.

26. Khalil V, Faress I, Mermet-Joret N, Kerwin P, Yonehara K, Nabavi S (n.d.): Subcortico-amygdala pathway processes innate and learned threats. *eLife* 12: e85459.

27. Root DH, Estrin DJ, Morales M (2018): Aversion or Salience Signaling by Ventral Tegmental Area Glutamate Neurons. *iScience* 2: 51–62.

28. Barbano MF, Wang H-L, Zhang S, Miranda-Barrientos J, Estrin DJ, Figueroa-González A, *et al.* (2020): VTA Glutamatergic Neurons Mediate Innate Defensive Behaviors. *Neuron*. https://doi.org/10.1016/j.neuron.2020.04.024

29. Taylor SR, Badurek S, DiLeone RJ, Nashmi R, Minichiello L, Picciotto MR (2014): GABAergic and Glutamatergic Efferents of the Mouse Ventral Tegmental Area. *J Comp Neurol* 522: 3308–3334.

Journal Pre-proof

30. Fernandez SP, Broussot L, Marti F, Contesse T, Mouska X, Soiza-Reilly M, *et al.* (2018): Mesopontine cholinergic inputs to midbrain dopamine neurons drive stress-induced depressive-like behaviors. *Nature Communications* 9: 4449.

31. Ortiz V, Costa Campos R, Fofo H, Fernandez SP, Barik J (2022): Nicotinic receptors promote susceptibility to social stress in female mice linked with neuroadaptations within VTA dopamine neurons. *Neuropsychopharmacol* 1–10.

32. Tye KM, Prakash R, Kim S-Y, Fenno LE, Grosenick L, Zarabi H, *et al.* (2011): Amygdala circuitry mediating reversible and bidirectional control of anxiety. *Nature* 471: 358–362.

33. Rainnie DG, Asprodini EK, Shinnick-Gallagher P (1993): Intracellular recordings from morphologically identified neurons of the basolateral amygdala [no. 4]. *Journal of Neurophysiology* 69: 1350–1362.

34. Duvarci S, Paré D (2007): Glucocorticoids Enhance the Excitability of Principal Basolateral Amygdala Neurons [no. 16]. *J Neurosci* 27: 4482–4491.

35. Linders LE, Supiot LF, Du W, D'Angelo R, Adan RAH, Riga D, Meye FJ (2022): Studying Synaptic Connectivity and Strength with Optogenetics and Patch-Clamp Electrophysiology [no. 19]. *International Journal of Molecular Sciences* 23: 11612.

36. Zheng N, Gui Z, Liu X, Wu Y, Wang H, Cai A, *et al.* (2023): Investigations of brain-wide functional and structural networks of dopaminergic and CamKIIα-positive neurons in VTA with DREADD-fMRI and neurotropic virus tracing technologies. *Journal of Translational Medicine* 21: 543.

37. Janak PH, Tye KM (2015): From circuits to behaviour in the amygdala [no. 7534]. *Nature* 517: 284–292.

38. McDonald AJ (1998): Cortical pathways to the mammalian amygdala. *Progress in Neurobiology* 55: 257–332.

Journal Pre-proof

39. Duvarci S, Pare D (2014): Amygdala Microcircuits Controlling Learned Fear [no. 5]. *Neuron* 82: 966–980.

40. Meye FJ, Valentinova K, Lecca S, Marion-Poll L, Maroteaux MJ, Musardo S, *et al.* (2015): Cocaine-evoked negative symptoms require AMPA receptor trafficking in the lateral habenula. *Nat Neurosci* 18: 376–378.

41. Liu J, Conde K, Zhang P, Lilascharoen V, Xu Z, Lim BK, *et al.* (2017): Enhanced AMPA Receptor Trafficking Mediates the Anorexigenic Effect of Endogenous Glucagon-like Peptide-1 in the Paraventricular Hypothalamus [no. 4]. *Neuron* 96: 897-909.e5.

42. Kuniishi H, Yamada D, Wada K, Yamada M, Sekiguchi M (2020): Stress induces insertion of calcium-permeable AMPA receptors in the OFC–BLA synapse and modulates emotional behaviours in mice [no. 1]. *Translational Psychiatry* 10: 1–11.

43. Rumpel S, LeDoux J, Zador A, Malinow R (2005): Postsynaptic Receptor Trafficking Underlying a Form of Associative Learning. *Science* 308: 83–88.

44. Malinow R, Malenka RC (2002): AMPA receptor trafficking and synaptic plasticity. *Annu Rev Neurosci* 25: 103–126.

45. Rumpel S, LeDoux J, Zador A, Malinow R (2005): Postsynaptic Receptor Trafficking Underlying a Form of Associative Learning [no. 5718]. *Science* 308: 83–88.

46. McCormack SG, Stornetta RL, Zhu JJ (2006): Synaptic AMPA Receptor Exchange Maintains Bidirectional Plasticity [no. 1]. *Neuron* 50: 75–88.

47. Calhoon GG, Tye KM (2015): Resolving the neural circuits of anxiety. *Nat Neurosci* 18: 1394–1404.

48. Tovote P, Fadok JP, Lüthi A (2015): Neuronal circuits for fear and anxiety. *Nat Rev Neurosci* 16: 317–331.

Journal Pre-proof

49. Beyeler A, Chang C-J, Silvestre M, Lévêque C, Namburi P, Wildes CP, Tye KM (2018): Organization of Valence-Encoding and Projection-Defined Neurons in the Basolateral Amygdala. *Cell Reports* 22: 905–918.

50. McDonald AJ (1985): Immunohistochemical identification of γ-aminobutyric acid-containing neurons in the rat basolateral amygdala. *Neuroscience Letters* 53: 203–207.

51. McDonald AJ (1982): Neurons of the lateral and basolateral amygdaloid nuclei: A golgi study in the rat. *Journal of Comparative Neurology* 212: 293–312.

52. Kim J, Pignatelli M, Xu S, Itohara S, Tonegawa S (2016): Antagonistic negative and positive neurons of the basolateral amygdala [no. 12]. *Nat Neurosci* 19: 1636–1646.

53. Wang DV, Wang F, Liu J, Zhang L, Wang Z, Lin L (2011): Neurons in the Amygdala with Response-Selectivity for Anxiety in Two Ethologically Based Tests. *PLOS ONE* 6: e18739.

54. Vyas A, Mitra R, Rao BSS, Chattarji S (2002): Chronic Stress Induces Contrasting Patterns of Dendritic Remodeling in Hippocampal and Amygdaloid Neurons. *J Neurosci* 22: 6810–6818.

55. Liu W-Z, Zhang W-H, Zheng Z-H, Zou J-X, Liu X-X, Huang S-H, *et al.* (2020): Identification of a prefrontal cortex-to-amygdala pathway for chronic stress-induced anxiety [no. 1]. *Nature Communications* 11: 1–15.

56. Zheng Z, Guo C, Li M, Yang L, Liu P, Zhang X, *et al.* (2022): Hypothalamus-habenula potentiation encodes chronic stress experience and drives depression onset. *Neuron* 110: 1400-1415.e6.

57. Christoffel DJ, Golden SA, Walsh JJ, Guise KG, Heshmati M, Friedman AK, *et al.* (2015): Excitatory transmission at thalamo-striatal synapses mediates susceptibility to social stress. *Nature Neuroscience* 18: 962–964.

58. Pape H-C, Pare D (2010): Plastic Synaptic Networks of the Amygdala for the Acquisition, Expression, and Extinction of Conditioned Fear. *Physiological Reviews* 90: 419–463.

59. Humeau Y, Reisel D, Johnson AW, Borchardt T, Jensen V, Gebhardt C, *et al.* (2007): A Pathway-Specific Function for Different AMPA Receptor Subunits in Amygdala Long-Term Potentiation and Fear Conditioning. *J Neurosci* 27: 10947–10956.

60. Faccidomo S, Cogan ES, Hon OJ, Hoffman JL, Saunders BL, Eastman VR, *et al.* (n.d.): Calcium-permeable AMPA receptor activity and GluA1 trafficking in the basolateral amygdala regulate operant alcohol self-administration. *Addiction Biology* n/a: e13049.

61. Cai Y-Q, Hou Y-Y, Pan ZZ (2020): GluA1 in central amygdala increases pain but inhibits opioid withdrawal-induced aversion. *Mol Pain* 16: 1744806920911543.

62. Hubert GW, Li C, Rainnie DG, Muly EC (2014): Effects of stress on AMPA receptor distribution and function in the basolateral amygdala. *Brain Struct Funct* 219: 1169–1179.

63. Schultz W (2016): Dopamine reward prediction-error signalling: a two-component response. *Nat Rev Neurosci* 17: 183–195.

64. Lammel S, Lim BK, Malenka RC (2014): Reward and aversion in a heterogeneous midbrain dopamine system. *Neuropharmacology* 76: 351–359.

65. Morel C, Montgomery SE, Li L, Durand-de Cuttoli R, Teichman EM, Juarez B, *et al.* (2022): Midbrain projection to the basolateral amygdala encodes anxiety-like but not depression-like behaviors [no. 1]. *Nat Commun* 13: 1532.

66. Nguyen C, Mondoloni S, Borgne TL, Centeno I, Come M, Jehl J, *et al.* (2021): Nicotine inhibits the VTA-to-amygdala dopamine pathway to promote anxiety. *Neuron* 109: 2604-2615.e9.

67. Chen S-Y, Yao J, Hu Y-D, Chen H-Y, Liu P-C, Wang W-F, *et al.* (2022): Control of Behavioral Arousal and Defense by a Glutamatergic Midbrain-Amygdala Pathway in Mice. *Front Neurosci* 16: 850193.

68. Broussot L, Contesse T, Costa-Campos R, Glangetas C, Royon L, Fofo H, *et al.* (2022): A non-canonical GABAergic pathway to the VTA promotes unconditioned freezing. *Mol Psychiatry* 1–13.

Figure Legends

Figure 1. Chronic social defeat increases anxiety, glutamate release and synaptic firing in basolateral amygdala principal neurons.

(A) Schematic experimental time line of CSD protocol followed by behavioural and electrophysiology characterization. **(B)** Exposure to CSD decreases exploration time in open arms (t=6.506, df=57) and open arm entries (t=5.920, df=57) in the O-maze test compared to control mice (n= 29 control and n=30 CSD, Student's t test, ***p < 0.001). **(C)** Exposure to CSD decreases exploration time in center zone (t=5.637, df=35) but no total distance travelled (t=1.707, df=35) in the open field test compared to control mice (n= 18 control and n= 19 CSD, Student's t test, ***p < 0.001). **(D)** Patch-clamp recordings in acute brain slices containing the BLA. CSD exposure did not significantly affect resting membrane potential (RMP, t=0.4643, df=27) or membrane resistance (Rm, t=1.221, df=27) of BLA principal neurons (n=14 control and n=15 CSD, Student's t test, ns: not significant). On the right, excitability curves to increasing current injection steps were not significantly different between control and CSD groups (F(9, 195) = 0.6282, n=14 control and n=15 CSD, two-way ANOVA treatment x current with repeated measures, ns: not significant). Representative voltage traces for each condition are shown on the far right. **(E)** The frequency but not the amplitude of isolated excitatory post-synaptic currents (EPSCs) onto BLA principal neurons is augmented after CSD compared to control (tampli=1.769 and tfreq=4.928, df=27n= 14 control and n= 15 CSD, Student's t test, ***p < 0.001, ns: not significant). Each panel depicts cumulative frequency distribution of total events and mean per condition (inset). Representative current traces per conditions are shown on the far right. **(F)** Synaptic stimulation to generate action potentials in BLA principal neurons. Three stimulation trains containing 5 pulses were delivered at 50Hz. Exposure to CSD increases the probability of discharge compared to control conditions (F(4, 120) = 10.36, n= 14 control and CSD= 18, two-way ANOVA with repeated measures

followed by Sidak's post-hoc test, ***p < 0.001). Representative voltage traces are depicted for each condition. All data are expressed as mean±SEM.

Figure 2. VTAGlu neurons make functional synapses onto BLA principal neurons

(A) VGluT2-Cre mice were injected with AAV-DIO-ChR2-mcherry in the VTA. Patch-clamp recording of BLA principal neurons was combined with optogenetic stimulation of VTAGlu axon terminals. Representative traces of light-evoked currents and action potentials in the BLA. Optical EPSCs were blocked by the perfusion of the AMPA antagonist DNQX (t=5.325, df=4, n=5, Student's paired t-testp<0.01). **(B)** In a subset of neurons, cytoplasm was aspirated in the pipette after electrophysiology recording was completed. This content was used to perform single-cell PCR for the glutamatergic markers VGluT1, VGluT2, and the GABAergic markers GAD65 and GAD67. An intron genomic control is run parallel to verified that the nucleus was not aspired during cytoplasm extraction (GEN). **(C)** Viral injection of AAV2-CaMKII-ChR2-mCherry into VTA, and AAV2-DIO-eYFP into BLA of vglut1-Cre mice to target BLA VGluT1 neurons. **(D)** Fluorescent micrographs showing VTAVGluT2 axon terminals (yellow arrows) co-expressing mCherry (red) and VGluT2 (white) making contacts on BLAVGluT1 somas or dendrites expressing eYFP (green, for BLA VGluT1 detection). High magnification images showing closer views of each channel and overlay for the yellow box in the low magnification image. **(E)** Electron micrograph showing an axon terminal (red outline) from VTAVGluT2 neurons co-expressing mCherry (scattered dark material) and VGluT2 (gold particles, red arrowhead) making an asymmetric synapse (green arrow) with a BLAVGluT1 dendrite (green outline) expressing eYFP (gold particles, green arrowhead, for VGluT1 detection). All data are expressed as mean±SEM.

Journal Pre-proof

Figure 3. VTAGlu→BLA neurons are activated by social stress

(A) VGluT2-Cre mice were injected with retrograde AAV-Flex-tdTomato in the BLA. Retrogradely labelled neurons were significantly higher in VTA medial (mVTA) vs lateral (lVTA) parts (t=5.258, df=10, n=5, Student's t-test, **p<0.01). VTAGlu BLA-projecting neurons did not express the dopaminergic marker tyrosine hydroxylase (TH). **(B)** VGluT2-Cre mice were injected with a retrograde AAV-Flex-TdTomato in the BLA. Three weeks later, mice were subjected to an acute social defeat session (5min) followed by 1h sensory contact with the aggressor. An immunostaining against cFos (green) and TH (blue) was performed. The number of VGluT2 retrogradelly-labelled neurons (red) co-labelled with cFos were significantly higher in the defeated group (t=2.559, df=9, n= 5 control, n= 6 defeat, Student's t test, *p < 0.05). **(C)** Fiber photometry recordings of GCAMP signals over VTAGlu neuron somas. Photo depicts an example of GCAMP8m expression and fiber placement. Representative recordings depicting Ca2+ responses evoked by defeat bouts. Peri-event plot of averaged responses to defeat bouts and signal quantification showing a significant increase in Ca2+ responses after defeats (t=4.844, df=8, n=9, paired Student's t test, **p < 0.01). **(D)** VGluT2-Cre mice were injected with a retrograde AAV-Flex-TdTomato in the BLA. Three weeks later, mice were subjected to CSD. 24 hours after the last social defeat session, mice anxious phenotype was confirmed in the O-maze (data not shown) and ex vivo electrophysiological recordings of BLA-projecting VTAGlu neurons was performed. Excitability was increased after CSD (F(6, 240) = 3.460, n= 21 control and n= 21 CSD, two-way ANOVA with repeated measures followed by Sidak's post-hoc test, ***p < 0.001). Representative voltage traces are shown for each condition.

Journal Pre-proof

Figure 4. Converging inputs from mPFC and VTA onto BLA neurons are selectively potentiated by CSD.

(A) Strategy used to record calcic responses in BLA neurons in response to mPFC and medial VTA stimulation. An anterograde trans-synaptic virus expressing Cre was injected in the mPFC and a cre-dependent virus expressing the calcium sensor GCaMP8f was injected in the BLA. Fiber photometry in anesthetized mice was performed 4 weeks later. The optic fiber was placed above the BLA and two stimulating electrodes in the mPFC and medial VTA. **(B)** Representative example of GCaMP expression and optic fiber placement in the BLA (top left), Cre expression and electrode placement in the mPFC (top right) and electrode placement in the medial VTA (bottom). **(C-D)** Mean changes in fluorescence following mPFC (c) or medial VTA (d) stimulation in a burst-like pattern (5 pulses of 10 or 20Hz every 2s - repeated 100 times) or continuous-like pattern (30s at 10 or 20Hz). Representative traces of mPFC and medial VTA 20Hz burst-like stimulation are shown, with the calcium-dependent signal (473nm, light blue) and isobestic signal (405nM, purple). Scale bar: 100um. Arrows illustrate time points of burst-like stimulations. Abreviations: mPFC: medial Prefrontal Cortex, BLA: Basolateral Amygdala, LA: Lateral Amygdala, IL: Infralimbic Cortex, PL: Prelimbic Cortex, Cg: Cingulate Cortex, VTA: Ventral Tegmental Area, SNc: Substantia nigra pars, compacta, SNr: Substantia nigra, pars reticulata, ACB: Nucleus Accumbens, LSr: Lateral septum, DP: Dorsal Peduncular Area, TT: Tenia Tecta, MO: Motor Cortex, TH: Tyrosine Hydroxylase. **(E)** Patch-clamp recordings in BLA principal neurons combined with light-evoked activation of mPFCGlu terminals. AMPA receptor to NMDA receptor ratio was not modified after CSD (t=0.5501, df=15, n= 8 control and n= 9 CSD, Student's t test). Representative traces of light-evoked EPSCs in BLA principal neurons at V= +40 mV in the absence or presence of DNQX (10 µM). **(F)** Patch-clamp recordings in BLA principal neurons combined with light-evoked activation of VTAGlu terminals. AMPA receptor to NMDA receptor ratio was significantly higher after CSD (t=2.247, df=14, n= 8 control and n= 8 CSD, Student's t

test, *p < 0.05). Representative traces of light-evoked EPSCs in BLA principal neurons at V= +40 mV in the absence or presence of DNQX (10 μM).

Figure 5. CSD potentiates VTAGlu-BLA connectivity via the insertion of AMPAR GluA1 subunits.

(A) VGluT2-Cre mice were injected with AAV-DIO-ChR2-mcherry in the VTA to perform patch-clamp recordings combined with optogenetic stimulation. **(B)** Current-voltage curves of AMPA receptor currents in BLA principal neurons after optogenetic stimulation of VTAGlu terminals. CSD increased rectification of AMPA receptor currents ($F(3, 63) = 3.591$, n= 13 control and n= 10 CSD, two-way ANOVA with repeated measures followed by Sidak's post-hoc test, *p < 0.05). Representative current traces at V=-70mV, 0mV, +40mV and +60mV for each condition. Rectification indices were calculated as current amplitude at -70 mV/amplitude at +60 mV ($t=2.286$, $df=21$, n= 13 control and n= 10 CSD, Student's t test, *p < 0.05). **(C)** Optogenetic stimulation of VTAGlu terminals to generate action potentials in BLA principal neurons. Three stimulation trains containing 5 pulses are delivered at 20Hz (left panel) or 50Hz (right panel). Exposure to CSD increases the probability of discharge compared to control conditions ($F(4, 152) = 18.96$ and $F(4, 152) = 8.327$, n= 18 control and CSD= 22, two-way ANOVA with repeated measures followed by Sidak's post-hoc test, ***p < 0.001). Representative voltage traces are depicted for each condition. **(D)** Representative image depicting staining of VTAGlu fibers (violet) and AMPA GluA1 subunits (green) in the BLA using high-resolution array tomography imaging. Yellow arrows: puncta apposition between VTAGlu axon terminals and GluA1-containing postsynaptic receptors. **(E)** Density of apposed puncta labeled for VTAGlu fibers and GluA1-containing receptors was significantly different in control vs CSD mice ($t=2.406$, $df=8$, n=5 control and n=5 CSD, Student's t test, *p < 0.05). All data are expressed as mean±SEM.

Figure 6. In vivo potentiation of VTAGlu synapses in the BLA promotes anxiety.

(A) Schematic illustration of the experimental timeline and representative image of fiber placement over the BLA. **(B)** 5-day in vivo optogenetic stimulation protocol significantly decreased exploration time in open arms (t=3.344, df=30) and open arm entries (t=2.560, df=30) in the O-maze test in ChR2 compared to control mice (n= 14 control and n= 18 ChR2, Student's t test, *p<0.05, **p < 0.01). Locomotor activity was not different between groups (t=0.7098, df=30, p=0.4833) **(C)** 5-day in vivo optogenetic stimulation produced a significant increase in AMPAR/NMDAR ratio VTAGlu synapses onto BLA principal neurons (t=2.560, df=16, n= 8 control and n= 10 ChR2, Student's t test, *p < 0.05). Representative traces of light-evoked EPSCs in BLA principal neurons at V= +40 mV in the absence or presence of DNQX (10 μM). **(D)** Current-voltage curves of AMPAR currents in BLA principal neurons after optogenetic stimulation of VTAGlu terminals. 5-day in vivo optogenetic stimulation produced a significant increase in AMPAR rectification (F(3, 45) = 3.110, n= 7 control and n= 10 ChR2, two-way ANOVA with repeated measures followed by Sidak's post-hoc test, *p < 0.05). Representative current traces at V=-70mV, 0mV, +40mV and +60mV for each condition. Rectification indices were calculated as current amplitude at -70 mV/amplitude at +60 mV (t=2.234, df=15, n= 7 control and n= 10 CSD, Student's t test, *p < 0.05).

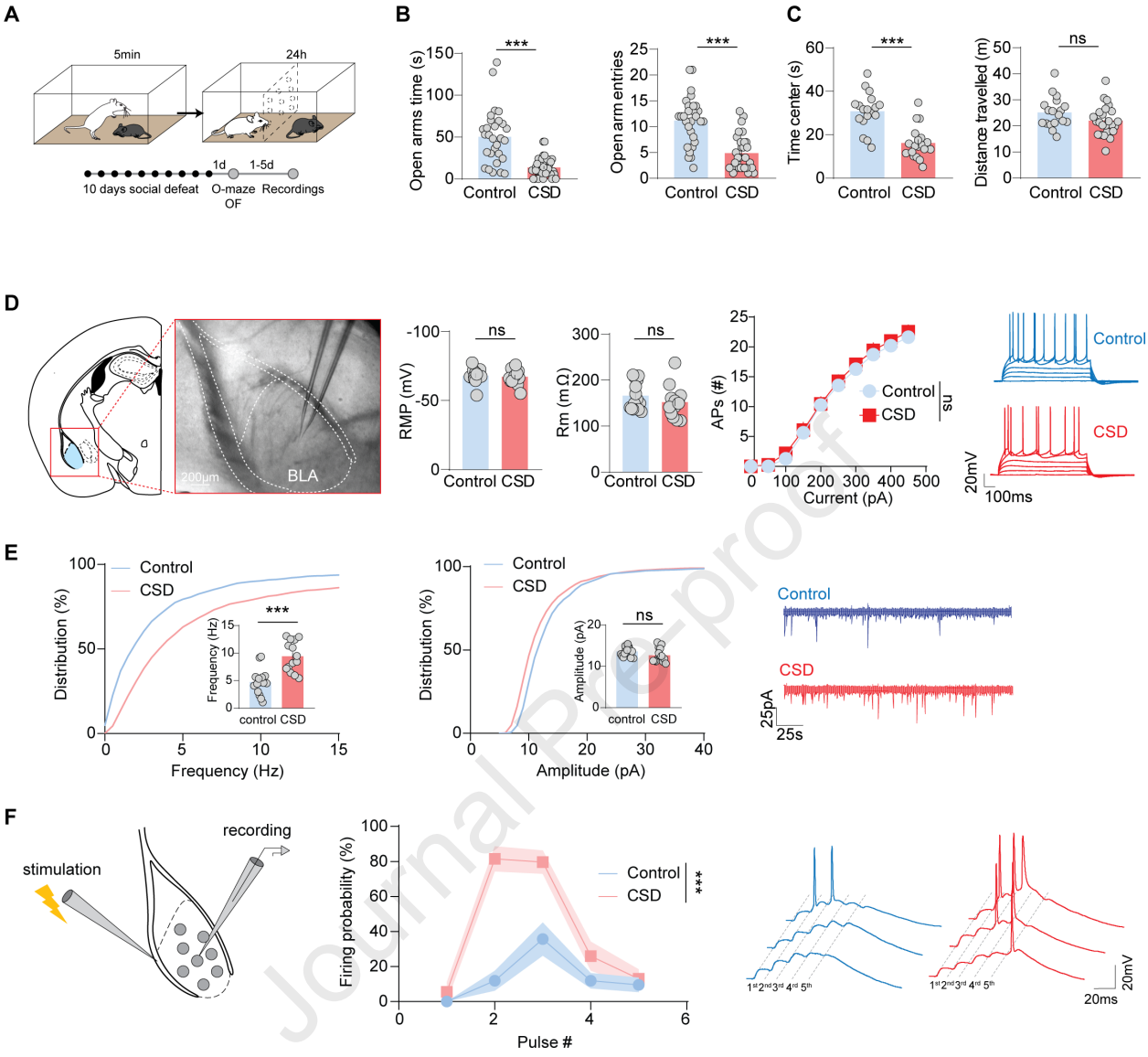
Figure 7. Blockade of AMPAR GluA1 subunit trafficking in VTA-BLA synapses prevents CSD-induced anxiety.

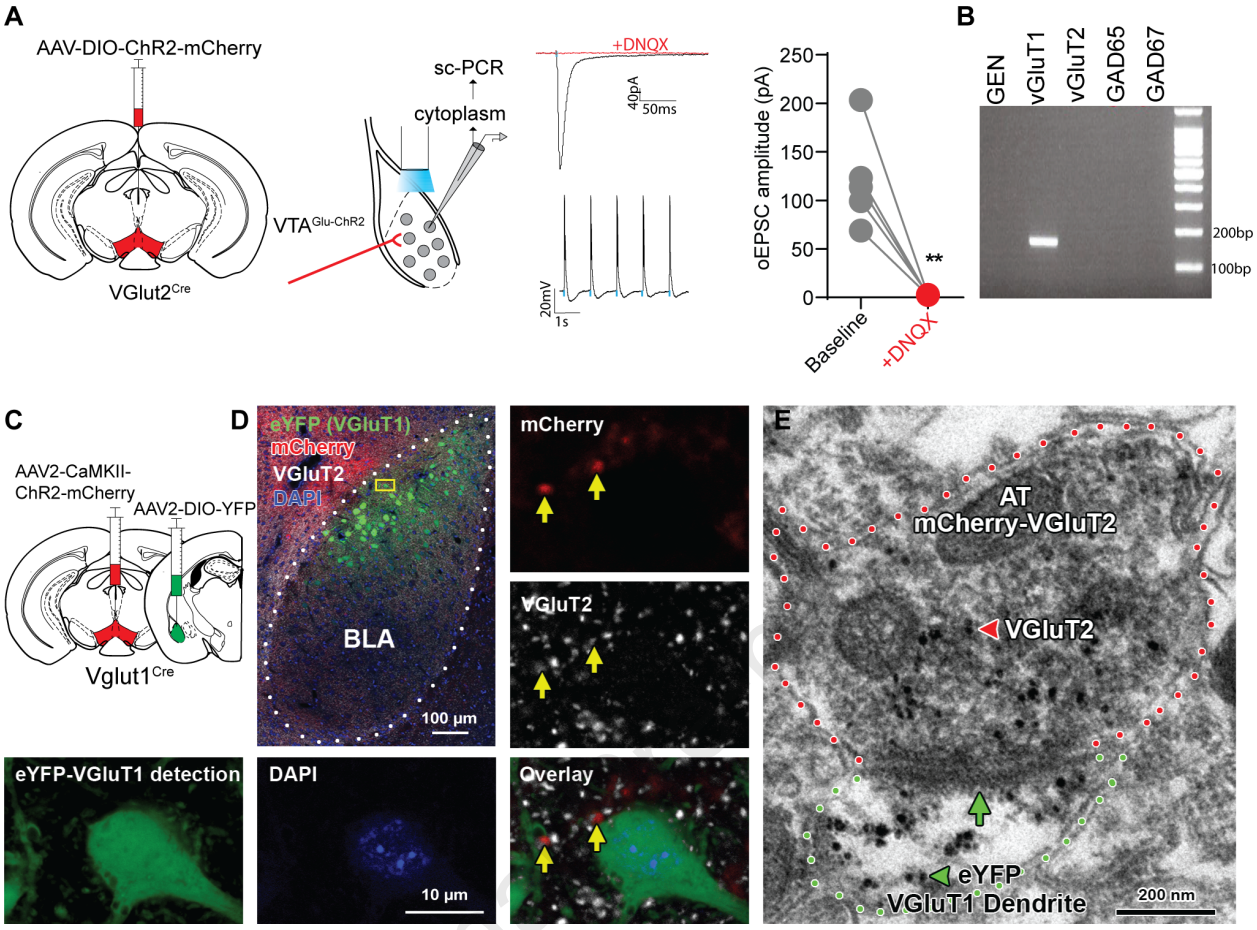
(A) Schematic representation showing AMPAR GluA1 subunits in the plasmatic membrane. A 81aminoacid c-terminal domain with mCherry tag is expressed to prevent insertion of AMPAR GluA1 subunits. **(B)** Schematic and timeline of experiments. WT mice were injected with trans-

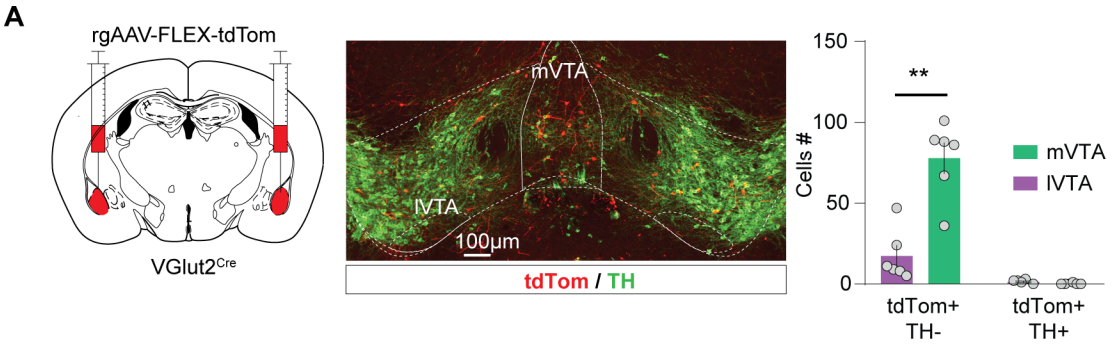
synaptic AAV1-CRE in the VTA and either AAV-DIO-mCherry (control) or AAV-DIOGluA1ct-mCherry (GluA1ct) in the BLA. Representative image showing the expression of GluA1ct-mCherry in BLA neurons that receive synaptic inputs from the VTA (anterior-posterior level -1mm). **(C)** In the O-maze, GluA1ct-mcherry expression significantly increased time in open arms ($F(1, 18) = 6.431$) and open arm entries ($F(1, 18) = 2.716$) in CSD mice (n= 10 control and n=10 GluA1ct-mCherry, two-way ANOVA with repeated measures followed by Sidak's post-hoc test, $^{**}p<0.01$, $^{*}p < 0.05$). **(D)** Time spent in the center ($F(1, 18) = 6.431$, $p=0.2239$) and total distance travelled ($F (1, 18) = 0.04636$, $p=0.8319$) in the open field test (n= 10 control and n=10 GluA1ct-mCherry, two-way ANOVA with repeated measures followed by Sidak's post-hoc test). (E) Patch-clamp recordings in mCherry-tagged neurons. Expression of GluA1ct did not affect membrane resting potential or membrane resistance compared to mCherry alone (n= 15 control and n=14 GluA1ct, Student's t test, ns: no significant). **(F)** Synaptic stimulation to generate action potentials in BLA principal neurons expressing mCherry (control) or GluA1ct. Three electrical stimulation trains containing 5 pulses are delivered at 50Hz. Exposure to CSD increases the probability of discharge in controls compared to GluA1ct ($F(4, 124) = 3.951$, n= 18 control and n= 15 GluA1ct, two-way ANOVA with repeated measures followed by Sidak's post-hoc test, $^{**}p < 0.01$). Representative voltage traces are depicted for each condition. All data are expressed as mean±SEM.

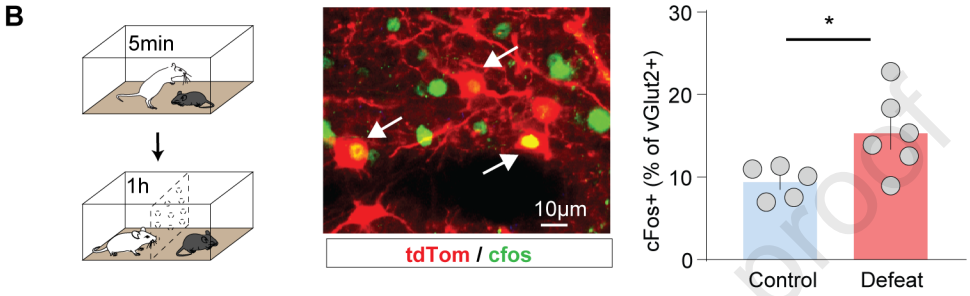
Journal Pre-proof

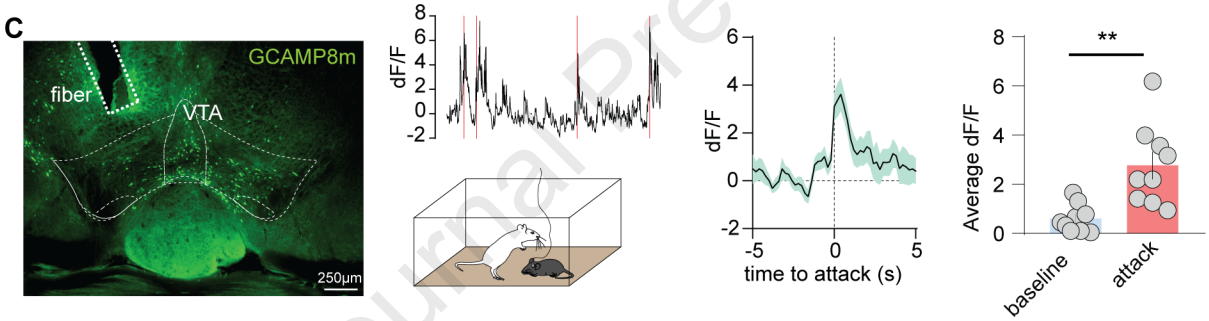
Journal Pre-proof

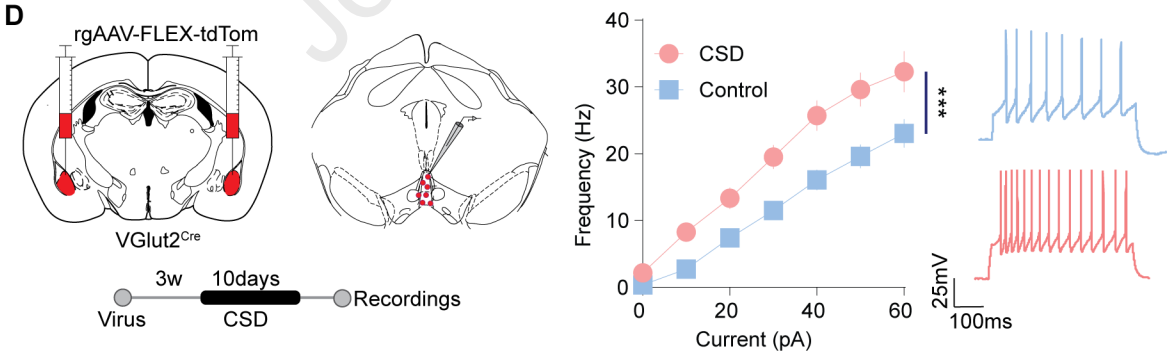



A
AAV-DIO-ChR2-mCherry
VGlut2Cre
VTAGlu-ChR2
sc-PCR
cytoplasm
+DNQX
40pA
50ms
20mV
1s
oEPSC amplitude (pA)
250
200
150
100
50
0
**
Baseline
+DNQX
B
GEN
vGluT1
vGluT2
GAD65
GAD67
200bp
100bp
C
AAV2-CaMKII-ChR2-mCherry
AAV2-DIO-YFP
Vglut1Cre
D
eYFP (VGluT1)
mCherry
VGluT2
DAPI
BLA
100 μm
mCherry
VGluT2
eYFP-VGluT1 detection
DAPI
10 μm
Overlay
E
AT
mCherry-VGluT2
VGluT2
eYFP
VGluT1 Dendrite
200 nm

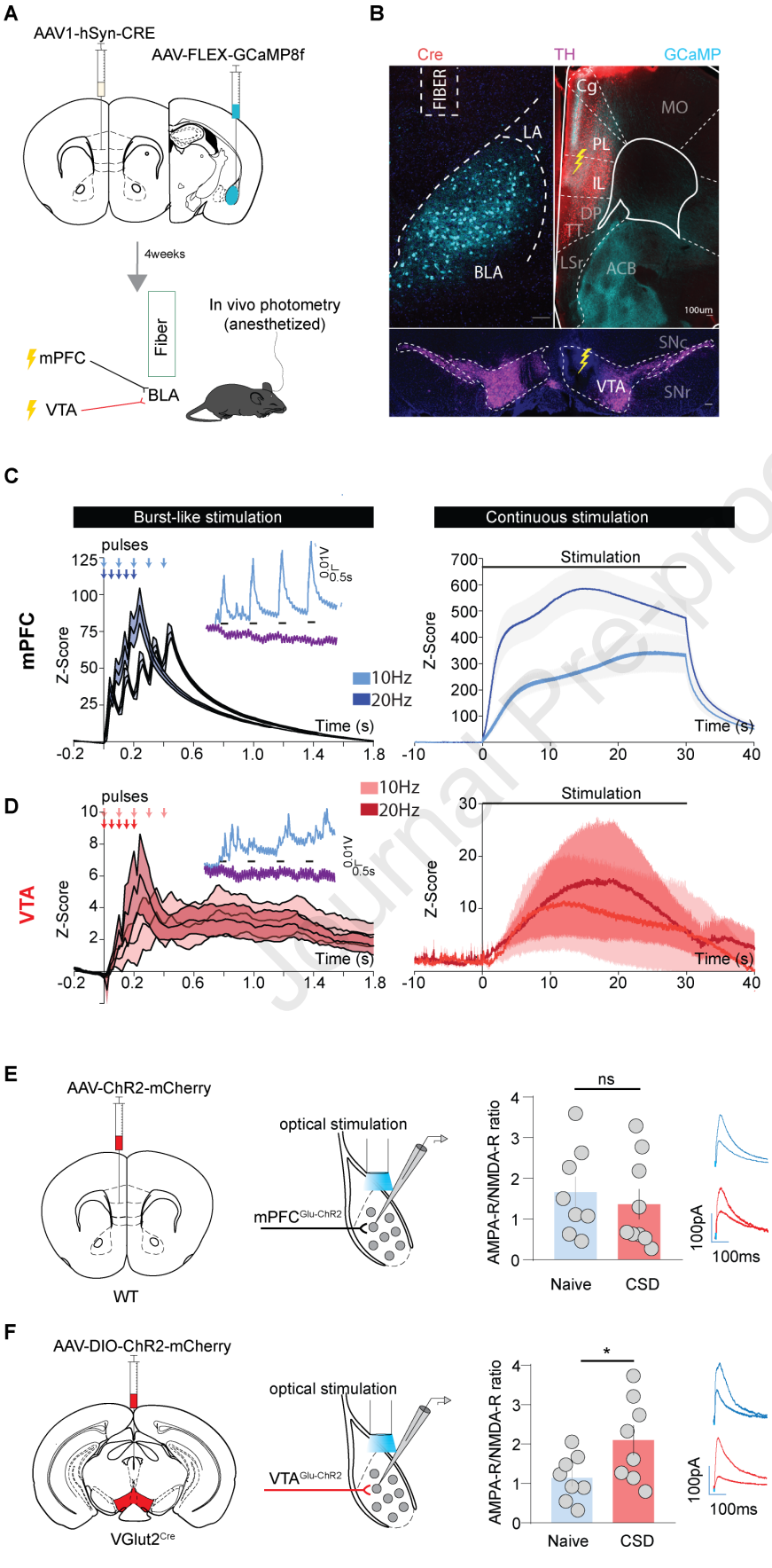


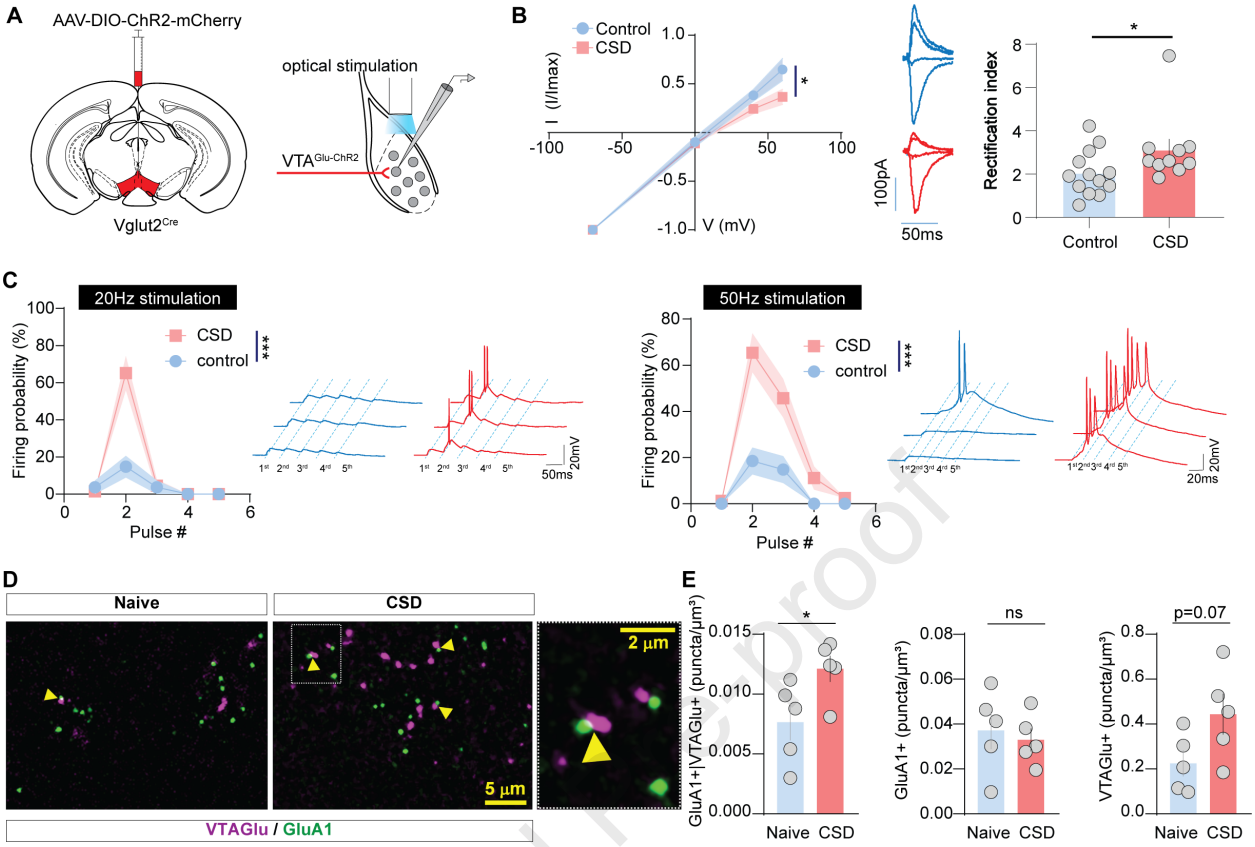






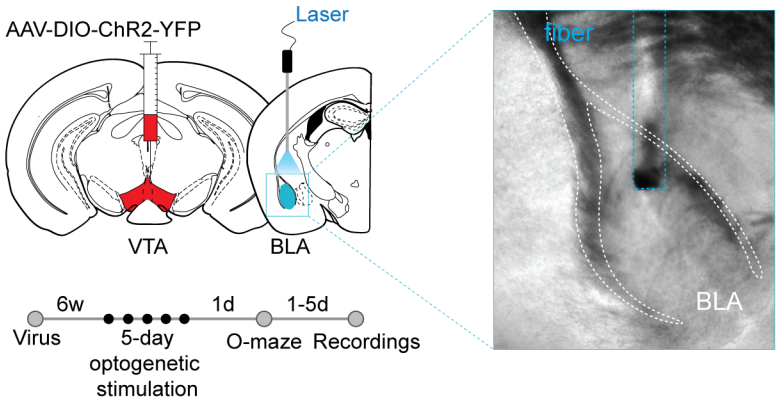
Journal Pre-proof


A
AAV1-hSyn-CRE
AAV-FLEX-GCaMP8f
4weeks
Fiber
In vivo photometry
(anesthetized)
mPFC
VTA
BLA
B
Cre
TH
GCaMP
FIBER
LA
BLA
Cg
MO
PL
IL
DP
TT
LSr
ACB
100um
SNc
VTA
SNr
C
Burst-like stimulation
Continuous stimulation
mPFC
pulses
Z-Score
Time (s)
10Hz
20Hz
0.01V
0.5s
Stimulation
D
VTA
E
AAV-ChR2-mCherry
WT
optical stimulation
mPFCGlu-ChR2
AMPA-R/NMDA-R ratio
ns
Naive
CSD
100pA
100ms
F
AAV-DIO-ChR2-mCherry
VGlut2Cre
optical stimulation
VTAGlu-ChR2
*
Naive
CSD
100pA
100ms

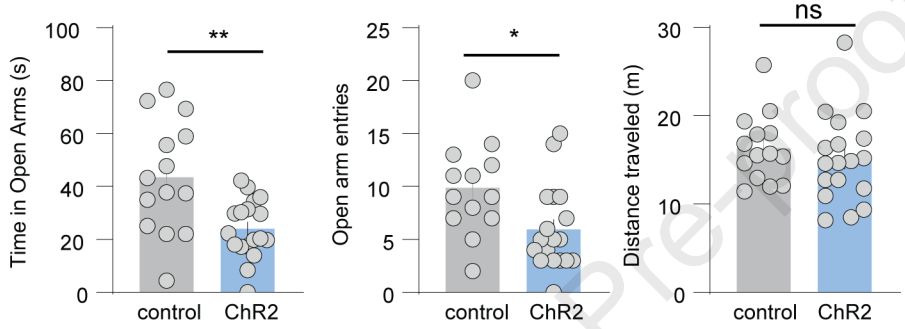


Journal Pre-proof

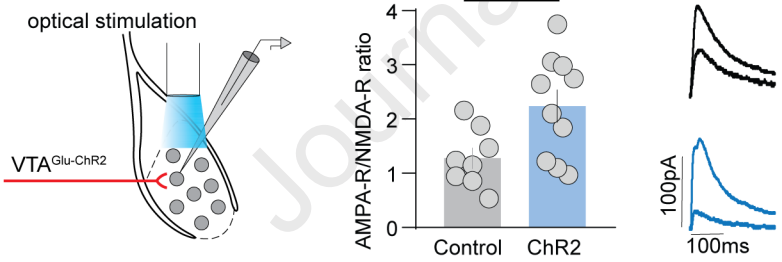
A



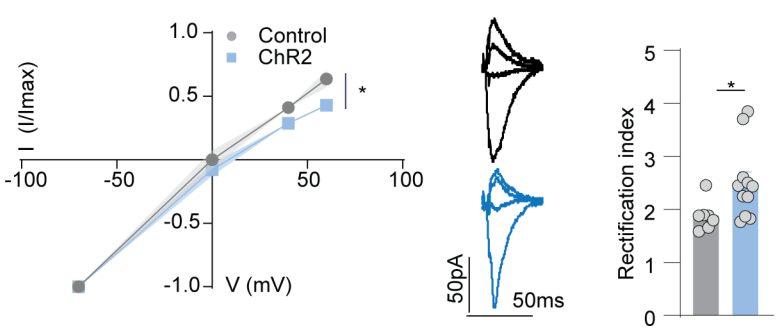
B



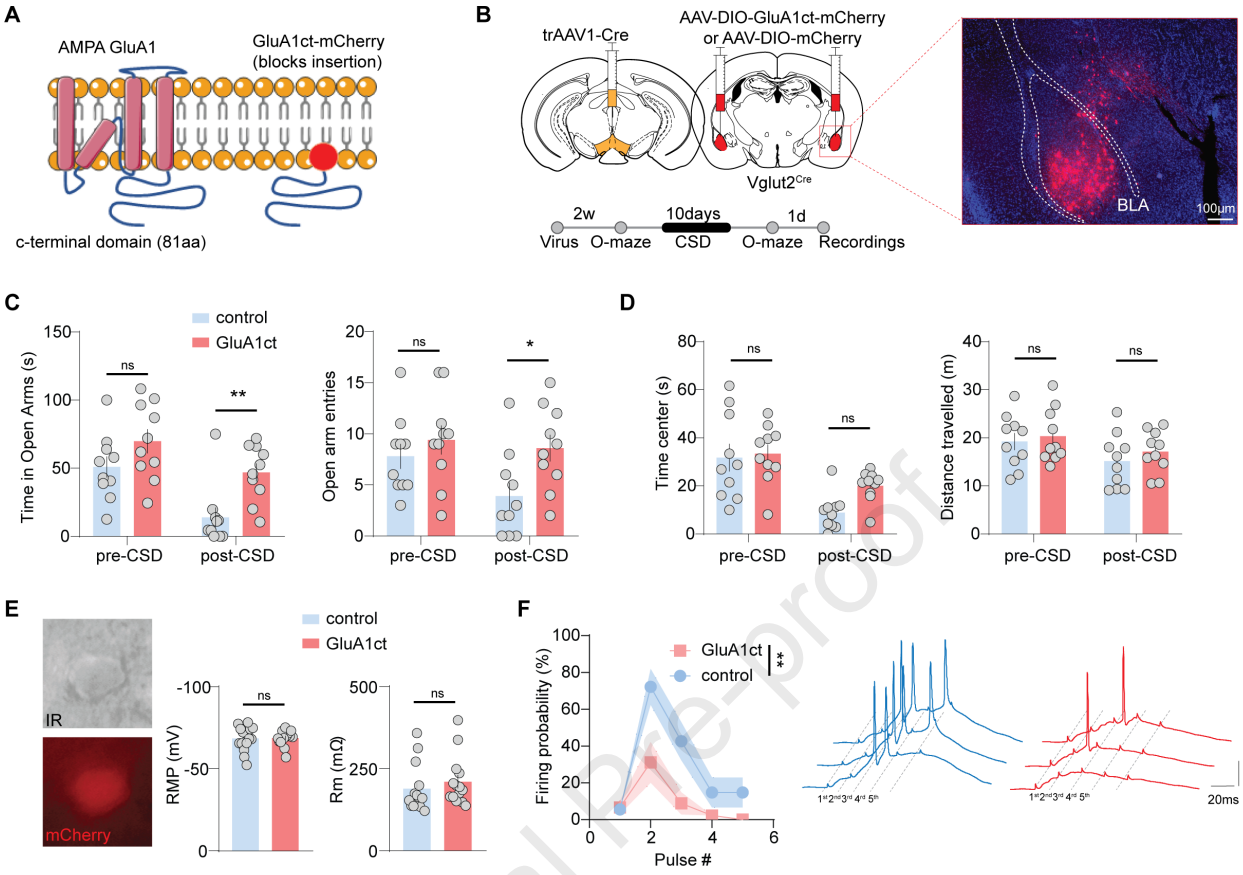
C



D



Journal Pre-proof



Journal Pre-proof